Assessment of MERIS reflectance data as processed with SeaDAS over the European seas

Frédéric Mélin,[1] Giuseppe Zibordi,[1] Jean-François Berthon,[1] Sean Bailey,[2,3] Bryan Franz,[3] Kenneth Voss,[4] Stephanie Flora,[5] and Mike Grant[6]

[1] *E.C. Joint Research Centre, TP272, via Fermi, 2749, Ispra, 21027, Italy*
[2] *Futuretech Corporation, 70307 Hanover Parkway, Greenbelt, Maryland 20771, USA*
[3] *Ocean Biology Processing Group 614.8, NASA Goddard Space Flight Center, Maryland 20771, USA*
[4] *University of Miami, Coral Gables, Florida 33124, USA*
[5] *Moss Landing Marine Laboratories, 8272 Moss Landing Road, California 95039, USA*
[6] *Plymouth Marine Laboratory, Prospect Place, The Hoe, Plymouth PL1 3DH*

frederic.melin@jrc.ec.europa.eu

Abstract: The uncertainties associated with MERIS remote sensing reflectance (R_{RS}) data derived from the SeaWiFS Data Analysis System (SeaDAS) are assessed with field observations. In agreement with the strategy applied for other sensors, a vicarious calibration is conducted using in situ data from the Marine Optical BuoY offshore Hawaii, and leads to vicarious adjustment factors departing from 1 by 0.2% to 1.6%. The three field data sets used for validation have been collected at fixed stations in the northern Adriatic Sea and the Baltic Sea, and in a variety of European waters in the Baltic, Black, Mediterranean and North Seas. Excluding Baltic waters, the mean absolute relative difference $|\psi|$ between satellite and field data is 10-14% for the spectral interval 490-560 nm, 16-18% at 443 nm, and 24-26% at 413 nm. In the Baltic Sea, the $|\psi|$ values are much higher for the blue bands characterized by low R_{RS} amplitudes, but similar or lower at 560 and 665 nm. For the three validation sets, the root-mean-square differences decrease from approximately 0.0013 sr^{-1} at 413 nm to 0.0002 sr^{-1} at 665 nm, and are found similar or lower than those obtained for SeaWiFS or MODIS-Aqua. As derived from SeaDAS, the R_{RS} records associated with these three missions thus provide a multi-mission data stream of consistent accuracy.

OCIS codes: (010.0010) Atmospheric and oceanic optics; (010.1285) Atmospheric correction; (280.4788) Optical sensing and sensors.

References and links

1. M. Rast, J. L. Bezy, and S. Bruzzi, "The ESA Medium Resolution Imaging Spectrometer MERIS - A review of the instrument and its mission," Int. J. Remote Sens. **20,** 1681–1702 (1999).
2. F. Mélin, "Merged series of normalized water leaving radiances obtained from multiple satellite missions for the Mediterranean Sea," Adv. Space Res. **43,** 423–437 (2009).
3. S. Djavidnia, F. Mélin, and N. Hoepffner, "Comparison of global ocean colour data records," Ocean Sci. **6,** 61–76 (2010).

4. F. Mélin, "Global distribution of the random uncertainty associated with satellite derived Chl*a*," IEEE Geosci. Remote Sens. Lett. **7,** 220–224 (2010).
5. F. Mélin, "Comparison of SeaWiFS and MODIS time series of inherent optical properties for the Adriatic Sea," Ocean Sci. **7,** 351–361 (2011).
6. G. Fu, K. S. Baith, and C. R. McClain, "The SeaWiFS Data Analysis System," in Proceedings of the 4th Pacific Ocean Remote Sensing Conference (Qingdao, China, July 1998), pp.73-79.
7. C. R. McClain, M. L. Cleave, G. C. Feldman, W. W. Gregg, S. B. Hooker, and N. Kuring, "Science quality SeaWiFS data for global biosphere research," Sea Tech. **39,** 10–16 (1998).
8. W. E. Esaias, M. R. Abbott, I. Barton, O. B. Brown, J. W. Campbell, K. L. Carder, D. K. Clark, R. H. Evans, F. E. Hoge, H. R. Gordon, W. M. Balch, R. Letelier, and P. J. Minnett, "An overview of MODIS capabilities for ocean science observations," IEEE Trans. Geosci. Remote Sens. **36,** 1250–1265 (1998).
9. D. K. Clark, H. R. Gordon, K. J. Voss, Y. Ge, W. Broenkow, and C. Trees, "Validation of atmospheric correction over the oceans," J. Geophys. Res. **102**, D14, 17209–17217 (1997).
10. S. W. Bailey, S. B. Hooker, D. Antoine, B. A. Franz, and P. J. Werdell, "Sources and assumptions for the vicarious calibration of ocean color satellite observations," Appl. Opt. **47**, 2035–2045 (2008).
11. S. W. Brown, S. J. Flora, M. J. Feinholz, M. A. Yarbrough, T. Houlihan, D. Peters, Y. S. Kim, J. L. Mueller, C. B. Johnson, and D. K. Clark, "The Marine Optical BuoY (MOBY) radiometric calibration and uncertainty budget for ocean color satellite sensor vicarious calibration," in *Sensors, Systems, and Next-Generation Satellites XI*, R. Meynart, S. P. Neeck, H. Shimoda, and S. Habib, eds., Proc. SPIE **6744**, pp. 67441M (2007).
12. A. Morel, D. Antoine, and B. Gentili, "Bidirectional reflectance of oceanic waters: accounting for Raman emission and varying particle scattering phase function," Appl. Opt. **41,** 6289–6306 (2002).
13. J. E. O'Reilly, S. Maritorena, D. A. Siegel, M. C. O'Brien, D. A. Toole, B. G. Mitchell, M. Kahru, F. P. Chavez, P. Strutton, G. F. Cota, S. B. Hooker, C. R. McClain, K. L. Carder, F. Mueller-Karger, L. Harding, A. Magnusson, D. Phinney, G. F. Moore, J. Aiken, K. R. Arrigo, R. Letelier, and M. Culver, "Ocean color chlorophyll a algorithms for SeaWiFS, OC2, and OC4: Version 4," in *NASA Technical Memorandum 2000-206892*, S.B. Hooker, and E.R. Firestone, eds., *20*, 9–23, (NASA-GSFC, Greenbelt, Maryland) (2000).
14. P. J. Werdell, "Ocean color chlorophyll (OC) v6," (2010), http://oceancolor.gsfc.nasa.gov/REPROCESSING/R2009/ocv6/
15. G. Zibordi, B. N. Holben, F. Mélin, D. D'Alimonte, J.-F. Berthon, I. Slutsker, and D. Giles, "AERONET-OC: An overview," Can. J. Remote Sens. **36,** 488–497 (2010).
16. G. Zibordi, F. Mélin, S. B. Hooker and B. N. Holben, "An autonomous above-water system for the validation of ocean color radiance data," IEEE Trans. Geosci. Remote Sens. **42**, 401–415 (2004).
17. G. Zibordi, B. N. Holben, I. Slutsker, D. Giles, D. D'Alimonte, F. Mélin, J.-F. Berthon, D. Vandemark, H. Feng, G. Schuster, B. E. Fabbri, S. Kaitala, and J. Seppälä, "AERONET-OC: A network for the validation of ocean color primary radiometric products," J. Atmos. Ocean. Tech. **26,** 1634–1651 (2009).
18. B. N. Holben, T. F. Eck, I. Slutker, D. Tanré, J. P. Buis, A. Setzer, E. Vermote, J. A. Reagan, Y. J. Kaufman, T. Nakajima, F. Lavenu, I. Jankowiak, A. Smirnov, "AERONET - A federated instrument network and data archive for aerosol characterization," Remote Sens. Environ. **66,** 1–16 (1998).
19. G. Zibordi, J.-F. Berthon, F. Mélin, and D. D'Alimonte, "Cross-site consistent in situ measurements for satellite ocean color applications: The BiOMaP radiometric dataset," Remote Sens. Environ. **115,** 2104–2115 (2011).
20. J.-F. Berthon, F. Mélin, and G. Zibordi, "Ocean colour remote sensing of the optically complex European seas," in *Remote Sensing of the European Seas*, V. Barale and M. Gade, eds. (Springer, 2008), pp.35-52.
21. G. Zibordi, and K. J. Voss, "Field radiometry and ocean color remote sensing," in *Oceanography from space, revisited*, V. Barale, L. Alberotanza, eds. (Springer, Dordrecht, Germany) pp. 365–398.
22. P. Goryl, J.-P. Huot, S. Delwart, M. Bouvet, E. Kwiatkowska, P. Regner, C. Lerebourg, C. Mazeran, L. Bourg, C. Brockmann, D. Antoine, B. Franz, G. Meister, C. Kent, J. Jackson, K. Barker, S. Lavender, R. Doerffer, J. Fischer, F. Zagolski, G. Zibordi, R. Santer, D. Ramon, J. Dash, and N. Gobron, "MERIS 3rd reprocessing," in *Proc. ESA Living Planet Symposium, ESA SP-686*, (Bergen, Norway, 28 June - 2 July 2010).
23. H. R. Gordon, and M. Wang, "Sensor-independent approach to the vicarious calibration of satellite ocean color radiometry," Appl. Opt. **46,** 5068–5082 (1994).
24. M. Wang, K. D. Knobelspiesse, and C. R. McClain, "Study of the Sea-viewing Wide Field-of-View Sensor (SeaWiFS) aerosol optical property data over ocean in combination with the ocean color products," J. Geophys. Res. **110,** D10S06, 10.1029/2004JD004950 (2005).
25. B. A. Franz, S .W. Bailey, P. J. Werdell, and C. R. McClain, "Sensor-independent approach to the vicarious calibration of satellite ocean color radiometry," Appl. Opt. **46,** 5068–5082 (2007).
26. Z. Ahmad, B. A. Franz, C. R. McClain, E. J. Kwiatkowska, P. J. Werdell, E. P. Shettle, and B. N. Holben, "New aerosol models for the retrieval of aerosol optical thickness and normalized water-leaving radiances from the SeaWiFS and MODIS sensors over coastal regions and open oceans," Appl. Opt. **49,** 5545–5560 (2010).
27. S. W. Bailey, B. A. Franz, and P. J. Werdell, "Estimation of near-infrared water-leaving reflectance for satellite ocean color data processing," Opt. Exp. **18,** 7521–7527 (2010).
28. L. Bourg, L. D'Alba, and P. Colagrande, "MERIS Smile Effect Characterization and Correction," ESA Technical Note, 2008, http://earth.eo.esa.int/pcs/envisat/meris/documentation/MERIS_Smile_Effect.pdf.
29. M. Wang, B. A. Franz, R. A. Barnes and C. R. McClain, "Effects of spectral bandpass on SeaWiFS-retrieved

near-surface optical properties of the ocean," Appl. Opt. **40**, 343–348 (2001).
30. G. Zibordi, F. Mélin, and J.-F. Berthon, "Comparison of SeaWiFS, MODIS and MERIS radiometric products at a coastal site," Geophys. Res. Lett. **33**, L06617, 10.1029/2006GL025778 (2006).
31. F. Mélin, G. Zibordi, and J.-F. Berthon, "Assessment of satellite ocean color products at a coastal site," Remote Sens. Environ. **110**, 192–215 (2007).
32. G. Zibordi, J.-F. Berthon, F. Mélin, D. D'Alimonte, and S. Kaitala, "Validation of satellite ocean color primary products at optically complex coastal sites: northern Adriatic Sea, northern Baltic Proper, Gulf of Finland," Remote Sens. Environ. **113**, 2574–2591 (2009).
33. R. M. Pope, and E. S. Fry, "Absorption spectrum (380-700nm) of pure water, II. Integrating cavity measurements," Appl. Opt. **36,** 8710–8723 (1997).
34. X. Zhang, L. Hu, and M.-X. He, "Scattering by pure seawater: Effect of salinity," Opt. Exp. **17,** 5698–5710 (2009).
35. J. M. Sullivan, M. S. Twardowski, R. V. Zaneveld, C. M. Moore, A. H. Barnard, P. L. Donaghay, and B. Rhoades, "Hyperspectral temperature and salt dependencies of absorption by water and heavy water in the 400-750 nm spectral range," Appl. Opt. **45,** 5294–5309 (2006).
36. S. W. Bailey, and P. J. Werdell, "A multi-sensor approach for the on-orbit validation of ocean color satellite data products," Remote Sens. Environ. **102,** 12–23 (2006).
37. F. Mélin, J.-F. Berthon, and G. Zibordi, "Assessment of apparent and inherent optical properties derived from SeaWiFS with field data," Remote Sens. Environ. **97,** 540–553 (2005).
38. H. Feng, D. Vandemark, J. W. Campbell, and B. N. Holben, "Evaluation of MODIS ocean colour products at a northeast United States coast site near the Martha's Vineyard Coastal Observatory," Int. J. Remote Sens. **29,** 4479–4497 (2008).
39. F. Mélin, M. Clerici, G. Zibordi, and B. Bulgarelli, "Aerosol variability in the Adriatic Sea from automated optical field measurements and SeaWiFS," J. Geophys. Res. **111,** D22201, 10.1029/2006JD007226 2006.
40. F. Mélin, M. Clerici, G. Zibordi, B. N. Holben, and A. Smirnov, "Validation of SeaWiFS and MODIS aerosol products with globally distributed AERONET data," Remote Sens. Environ. **114,** 230–250 (2010).
41. F. Mélin, G. Zibordi, and S. Djavidnia, "Development and validation of a technique for merging satellite derived aerosol optical depth from SeaWiFS and MODIS," Remote Sens. Environ. **108**, 436–450 (2007).
42. S. B. Hooker, and C. R. McClain, "The calibration and validation of SeaWiFS data," Prog. Oceanogr. **45**, 427–465 (2000).
43. H. R. Gordon, "Calibration requirements and methodology for remote sensors viewing the ocean in the visible," Remote Sens. Environ. **22**, 103–126 (1987).
44. H. R. Gordon, "In-orbit calibration strategy for ocean color sensors," Remote Sens. Environ. **63**, 265–278 (1998).
45. J.-F. Berthon, and G. Zibordi, "Optically black waters in the northern Baltic Sea," Geophys. Res. Lett. **37**, L09605, 10.1029/2010GL043227 (2010).
46. C. Jamet, H. Loisel, C. P. Kuchinke, K. Ruddick, G. Zibordi, and H. Feng, "Comparison of three SeaWiFS atmospheric correction algorithms for turbid waters using AERONET-OC measurements," Remote Sens. Environ. **115**, 1955–1965 (2011).
47. F. Mélin, and G. Zibordi, "Vicarious calibration of satellite ocean color sensors at two coastal sites," Appl. Opt. **49**, 798–810 (2010).
48. T. Schroeder, I. Behnert, M. Schaale, J. Fischer, and R. Doerffer, "Atmospheric correction algorithm for MERIS above case-2 waters," Int. J. Remote Sens. **28**, 1469–1486 (2007).
49. D. Antoine, F. d'Ortenzio, S. B. Hooker, G. Bécu, B. Gentili, D. Tailliez, and A. J. Scott, "Assessment of uncertainty in the ocean reflectance determined by three satellite ocean color sensors (MERIS, SeaWiFS and MODIS-A) at an offshore site in the Mediterranean Sea (BOUSSOLE project)," J. Geophys. Res. **113**, C07013, 10.1029/2007JC004472 (2008).
50. T. Cui, J. Zhang, S. Groom, L. Sun, T. Smyth, and S. Sathyendranath, "Validation of MERIS ocean-color products in the Bohai Sea: A case study for coastal waters," Remote Sens. Environ. **114**, 2326–2336 (2010).
51. C. Lerebourg, C. Mazeran, J.-P. Huot, D. Antoine, L. Bourg, S. Delwart, M. Ondrusek, S. Lavender, and P. Goryl, "MERIS vicarious adjustment in the near infrared and visible", in *Proc. Ocean Optics XX* (Anchorage, U.S., 27 Sep. - 1 Oct., 2010).
52. D. Antoine, P. Guevel, J.-F. Desté, G. Bécu, F. Louis, A. J. Scott, and P. Bardey, "The "BOUSSOLE" buoy - A new transparent-to-swell taut mooring dedicated to marine optics: Design, tests, and performance at sea," J. Atmos. Ocean. Tech. **25**, 968–989 (2008).
53. F. Mélin, and G. Zibordi, "An optically-based technique for producing merged spectra of water leaving radiances from ocean color," Appl. Opt. **46**, 3856–3869 (2007).
54. S. Maritorena, O. Hembise Fanton d'Andon, A. Mangin, and D. A. Siegel, "Merged satellite ocean color data products using a bio-optical model: Characteristics, benefits and issues," Remote Sens. Environ. **114**, 1791–1804 (2010).

1. Introduction

Considering the potential offered by ocean color remote sensing to investigate marine ecosystems, several space agencies have placed optical sensors in space during the last 15 years. The Medium Resolution Imaging Spectrometer (MERIS, [1]) was launched on-board the Envisat platform by the European Space Agency (ESA) on 1st March 2002, and has since provided global coverage of the biosphere with observations acquired at 15 spectral bands in the visible and near-infrared (NIR).

Even though the time series derived from the various ocean color missions are in general consistent, these satellite products show varying levels of differences (e.g., [2, 3, 4, 5]), that result from a complex set of factors, including different instrument designs, calibration strategies, atmospheric correction schemes, or bio-optical algorithms. An approach to minimize these differences is to adopt as many common elements as possible for the processing of the data streams. The SeaWiFS Data Analysis System (SeaDAS, [6]) developed by the National Aeronautics and Space Administration (NASA) offers the possibility of processing satellite ocean color imagery from various missions in a common framework, and has been extensively applied to imagery collected by the Sea-viewing Wide Field-of-View Sensor (SeaWiFS, [7]) and the Moderate Resolution Imaging Spectroradiometer (MODIS, on-board the platforms Terra and Aqua [8]).

This work investigates the application of SeaDAS to process MERIS data with a focus on European seas. After introducing the data used for the analysis, the vicarious calibration of MERIS is presented. Then, the uncertainties associated with MERIS-derived reflectance spectra are documented through comparison with field data collected in European waters.

2. Field and satellite data

2.1. MOBY data

The site used for vicarious calibration is the Marine Optical BuoY (MOBY) operating in deep oligotrophic waters offshore Lanai (Hawaii, [9]), which offers suitable environmental conditions [10] and accurate measurements [11] for that task. Water leaving radiance (or alternatively reflectance) values are derived from underwater hyper-spectral radiometric measurements (340-955 nm) at fixed depths along with above-water solar incident irradiance, and are convolved with the spectral response of the satellite sensor to yield MERIS-like radiance values. Bidirectional effects (dependence on illumination condition and seawater optical anisotropy) can be accounted for with look-up tables dependent on the chlorophyll *a* concentration [12], in turn computed from remote sensing reflectance with the standard empirical algorithm OC4v6 [13, 14]. The measurement series up to deployment 238 (September 2007) constitutes a consolidated set of radiometric data also used for vicarious calibration of SeaWiFS and MODIS, and is adopted here.

2.2. Field data in European seas

Radiometric field measurements for validation have been collected through two different sources. Autonomous observations are obtained at sites included in the Ocean Color component of the Aerosol Robotic Network (AERONET-OC, [15]), the Acqua Alta Oceanographic Tower (AAOT) in the northern Adriatic Sea, the Gustav Dalén Lighthouse Tower (GDLT) in the Baltic Proper, and the Helsinki Lighthouse Tower (HLT) in the Gulf of Finland (see Fig. 1 for positions). These sites operate the SeaWiFS Photometer Revision for Incident Surface Measurements (SeaPRISM [16]), a CE-318 sunphotometer (CIMEL Electronique, Paris, France) that performs sea-viewing radiance measurements following a common protocol [17]. At AAOT, continuous data collection started in April 2002, while at GDLT and HLT data have been col-

lected in the summer season (approximately April-May to September-October) since 2005 and 2006, respectively.

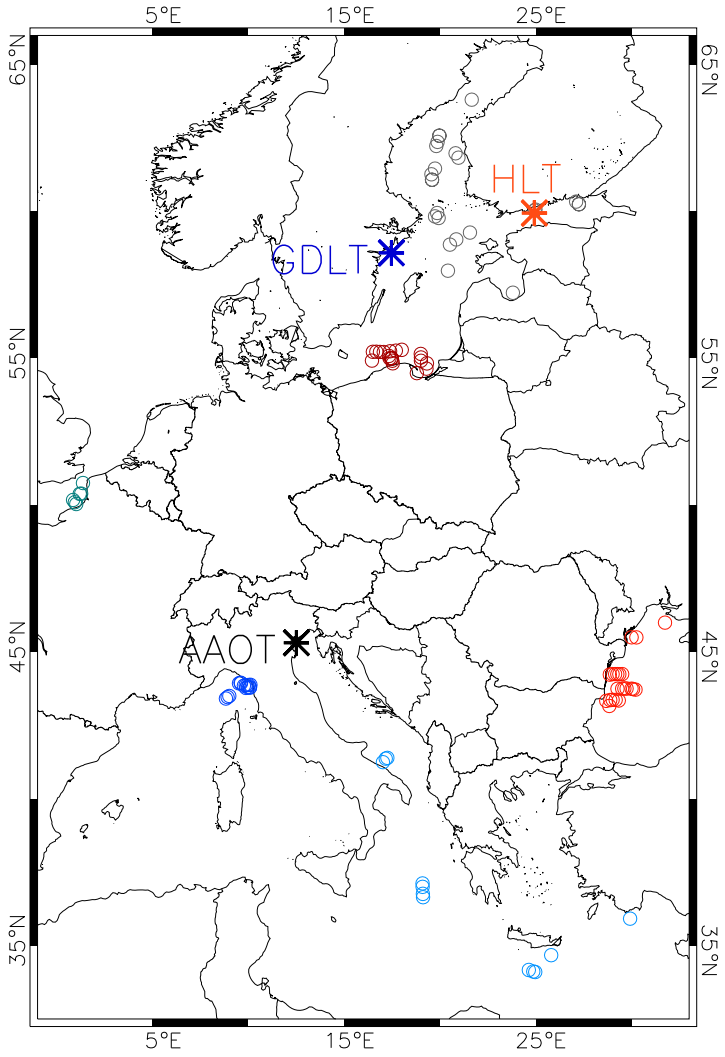

Fig. 1. Location of AAOT, GDLT, HLT, and match-ups obtained with the BiOMaP data set

The derived product of interest for the current work is the spectrum of remote sensing reflectance $R_{RS}(\lambda)$ at center-wavelengths close to those of the satellite ocean color sensors (see also Section 2.3 for a more complete definition of R_{RS}). This quantity is proportional to the normalized water leaving radiance, with the normalization entailing a correction for bidirectional effects [12]. All data are so-called Level-2 records, for which final calibration and quality checks have been applied. An uncertainty budget conducted at the AAOT site led to uncertainties of $\sim$5% in the blue-to-green spectral domain and $\sim$8% in the red [17]. As with regular

AERONET sites [18], direct solar irradiance measurements are used to derive the aerosol spectral optical thickness $\tau_a(\lambda)$, from which the Ångström exponent α is computed. The procedure to derive τ_a data is independent from that followed for R_{RS}, and on average, there are more τ_a data that fulfill the related AERONET quality checks. Validation results will be illustrated separately for the AAOT site, representative of a coastal environment with a moderate influence of sediments and dissolved organic matter, and for the two Baltic sites that are more characteristic of highly absorbing waters.

These autonomous measurement systems are optimal to gather validation data with regular frequency but they are tied to fixed locations. They are ideally supported by observations collected during ship campaigns that provide a more extensive view of various water bodies. The Bio-Optical mapping of Marine Properties (BiOMaP) program [19] has constructed a highly consistent data set of apparent and inherent optical properties (AOPs and IOPs, respectively) since 2004 (without counting the first proof-of-concept campaign in 2000). The measurement stations cover a significant part of the variability in optical conditions found in European seas, from oligotrophic to very turbid waters ([20], Fig.1), and has proved useful for the validation of satellite products [19]. In this case, the values of R_{RS} are derived from radiometric in-water profiles with center-wavelengths of 412, 443, 490, 510, 555 and 665 nm. Their uncertainties are estimated as $\sim$5% in the blue-to-green and $\sim$7% in the red [19, 21]. These data are accompanied by the determination of the chlorophyll *a* concentration (Chl*a*) and a comprehensive set of IOP measurements, including the absorption coefficients by pigmented particles, a_{ph}, non-pigmented particles, a_{npp}, and chromophoric dissolved organic matter (CDOM), a_{cdom}, and the backscattering coefficient of particles b_{bp}.

2.3. MERIS data and processing

MERIS data used in the present work are Level-1b top-of-atmosphere (TOA) radiance measurements resulting from the MERIS 3^{rd} reprocessing [22], for which the calibration history has been revisited. These data have then been processed with SeaDAS (version 6.2) with an atmospheric correction scheme originally devised by Gordon and Wang [23]. The scheme has known numerous evolutions [24, 25], including an updated set of aerosol models [26] and bio-optical modelling in the NIR [27]. The output of the atmospheric correction is the spectrum $R_{RS}(\lambda)$ at 413, 443, 490, 510, 560, 620, 665 and 681 nm, which is directly comparable to the field data. Two other channels, at 754 and 865 nm, are used for the selection of aerosol models and the determination of the aerosol optical thickness. The τ_a spectrum serves to compute the Ångström exponent α.

Following Franz et al. [25], the top-of-atmosphere radiance at wavelength λ, $L_t(\lambda)$ is written as (with dependencies other than λ omitted):

$$L_t(\lambda) = [L_r(\lambda) + L_a(\lambda) + t_{d_v}(\lambda)L_f(\lambda) + t_{d_v}(\lambda)L_w(\lambda)]t_{g_v}(\lambda)t_{g_s}(\lambda)f_p(\lambda) \quad (1)$$

where L_r, L_a, and L_f are the radiance contributed by air molecules in the absence of aerosols (Rayleigh scattering), aerosols (including their interactions with air molecules) and sea foam, respectively. The term t_{d_v} is the diffuse transmittance for the atmospheric path from sea surface to sensor; t_{g_v} and t_{g_s} represent the gaseous transmittance from the sea surface to the sensor and from the sun to the surface, respectively. Finally, f_p is a term correcting for polarization effects. The main output of the atmospheric correction scheme is the water leaving radiance L_w. Contributions from sun glint and correction of the so-called smile effect [28] are excluded from Equation 1.

The terms L_w and R_{RS} are related by:

$$R_{RS}(\lambda) = L_w(\lambda)/(\ _s f_s F_s(\lambda)t_{d_s}(\lambda)f_b(\lambda)f_\lambda(\lambda)) \quad (2)$$

where $_s$ is the cosine of the solar zenith angle θ_s, F_s is the extra-terrestrial solar irradiance, f_s is a correction for the variations in the sun-Earth distance, $t_{d_s}(\lambda)$ is the diffuse transmittance for the path from the sun to the sea surface, with these terms jointly operating a normalization by the solar illumination. The factor $f_b(\lambda)$ accounts for bidirectional effects [12], and f_λ corrects out-of-band contributions to L_w[29].

The field data are acquired at center wavelengths which are slightly different than those of MERIS. For a direct comparison between field and satellite values of R_{RS}, a band shift correction is performed on the field value when their center wavelengths differ by a few nm. The field value $R_{RS}(\lambda_0)$ is expressed at λ as follows:

$$R_{RS}(\lambda) = R_{RS}(\lambda_0)\frac{f(\lambda)}{Q(\lambda)}.\frac{Q(\lambda_0)}{f(\lambda_0)}.\frac{b_b(\lambda)}{a(\lambda)}.\frac{a(\lambda_0)}{b_b(\lambda_0)} \tag{3}$$

This approach has been already described in various studies (e.g., [30, 31]), and is only briefly introduced here. R_{RS} is considered a function of b_b/a, ratio of total backscattering and absorption, f, that relates the underwater irradiance reflectance to the ratio b_b/a, and Q, the ratio of underwater irradiance and radiance. The bidirectional effects having been corrected, f and Q are expressed with null solar and viewing zenith angles [12]. The absorption coefficient a is written as the sum a_w+a_{ph}+a_{npp}+a_{cdom}, and b_b as b_{bw}+b_{bp}, with a_w and b_{bw} absorption and backscattering associated with pure water, respectively. The values of Chl*a* (input to f/Q tables [12]) and IOPs at specific wavelengths are derived from regional empirical algorithms in the case of the AERONET-OC sites [32], whereas they are determined from field data in the case of the BiOMaP stations [19]. The IOPs of the various components are expressed at other wavelengths using assumed spectral shapes [32, 19]. For the AERONET-OC sites, a_w is a fixed spectrum [33], and b_{bw} has been computed with a salinity of 35 and 7 psu for AAOT and the Baltic sites, respectively [34]. For the BiOMaP data, a_w and b_{bw} are varied as a function of the salinity and temperature measured in situ [33, 35, 34].

Considering the wavelengths associated with field measurements, validation will be presented for R_{RS} at wavelengths in the interval 413 to 665 nm. If a SeaPRISM record lacks the band at 500 nm (a channel only included in the early SeaPRISM systems), the associated synthetic R_{RS} at 510 nm is not computed, leading to fewer match-ups at AAOT with respect to the other wavelengths, and to few match-ups for GDLT and HLT (so that the results for 510 nm are not presented for these 2 sites). As opposed to the data from AERONET-OC and BiOMaP utilized for validation activities, MOBY data employed for vicarious calibration do not require band-shift corrections because they are derived from hyper-spectral measurements combined with the spectral response of each MERIS band (see Section 2.1).

2.4. Match-up selection protocol for validation

The MERIS scenes at the locations of field observations are processed and a square of 3x3 pixels is extracted for analysis from the Level-2 files. The average R_{RS} computed over this macro-pixel is deemed the most representative value for comparison with the field observation. A match-up (i.e., concurrent field and satellite data) is retained for validation if it satisfies the following selection criteria: *i)* the time difference between satellite over-pass and field measurement is within an interval $\pm\Delta$t, *ii)* none of the 9 pixels is affected by the standard flags of the processing code which mostly exclude an atmospheric correction code failure, cloud, Sun glint or stray light conditions and high solar or viewing zenith angles [36], *iii)* R_{RS} averaged over the macropixel is higher than 0 at all channels, and *iv)* the coefficient of variation (CV, ratio of standard deviation and average) of the MERIS R_{RS} at selected wavelengths is lower than a threshold arbitrarily set to 20% [37, 38]. The bands selected for the CV test are those between 490 and 560 nm, wavelengths associated with a significant R_{RS} signal across most natural waters (whereas

R_{RS} can be near 0 in the blue and red domains for CDOM-dominated and oligotrophic waters, respectively). The value of Δt for the different data sets is a compromise between the requirement of obtaining a significant number of match-ups, the number of measurements available during the day at a given location (there are potentially multiple SeaPRISM observations at the AERONET-OC sites), and the general conditions found at the measurement sites. It is set to 2-h for the AERONET-OC sites (if several observations are available within the interval Δt, the closest record is selected for validation), and to 6-h for the BiOMaP set. In the latter case, Δt is large, particularly for coastal waters, but this is justified to encompass field measurements collected in the afternoon (MERIS overpass time is early in the morning) and thus obtain a fairly large match-up set; moreover, tests with Δt of 3 or 4-h do not significantly affect the average validation statistics (see Section 4.3).

The match-up selection protocol is slightly modified when comparing satellite and field aerosol products. First Δt is set to $\pm$1-h (as used in some previous works [38, 39, 40]) and there needs to be at least 2 AERONET measurements within that time window. The test on the CV is conducted on the aerosol optical thickness for the satellite $\tau_a(865)$ in space (i.e., applied to the 3x3-pixels of the satellite τ_a) and for the AERONET $\tau_a(870)$ in time (i.e., applied to the field data collected in the $\pm\Delta$t 2-h interval). In comparing satellite and field τ_a data, differences in center wavelengths are corrected using a 2^{nd}-order polynomial approximation for the τ_a spectrum [41].

Once the ensemble of N match-ups is selected, the differences between MERIS, x^M, and field values x^f are quantified by:

$$|\psi| = 100\frac{1}{N}\sum_{i=1}^{N}\frac{|x_i^M - x_i^f|}{x_i^f} \tag{4}$$

$$\psi = 100\frac{1}{N}\sum_{i=1}^{N}\frac{x_i^M - x_i^f}{x_i^f} \tag{5}$$

with $|\psi|$ and ψ respectively the mean absolute relative difference and mean relative difference (or bias) given in percent. The root-mean-square difference (*rmsd*) is also computed:

$$rmsd = \sqrt{\frac{1}{N}\sum_{i=1}^{N}(x_i^M - x_i^f)^2} \tag{6}$$

providing a measure of the uncertainty of R_{RS} in units of remote sensing reflectance (sr^{-1}).

3. Vicarious calibration

Considering R_{RS} accuracy goals (as low as 5% in clear waters [42]) and the generally small contribution of the water leaving radiance to the TOA radiance budget (usually smaller than 10%), vicarious calibration aims to adjust the system sensor+atmospheric correction scheme, by removing residual uncertainties associated with the calibration of the sensor in space and the modeling of the radiative transfer processes in the atmosphere [43, 44]. As a corollary, the resulting vicarious calibration coefficients are valid only for the considered sensor and code.

Vicarious calibration for MERIS is conducted, as for SeaWiFS and MODIS [25], by forcing Eq. (1) to reproduce the field value of the water leaving radiance L_w for each match-up i selected for the task. This is done for each band in the visible by introducing a multiplicative factor g_i for the TOA radiance L_t, called vicarious gain or adjustment factor (this implicitly treats the sensor as an integrated system combining its various constituents). The final vicarious adjustment factor is taken as the average $\overline{g}$ computed over the semi-interquartile range (SIQR) of the

Table 1. Vicarious Calibration Coefficients in the Visible for MERIS (N=102).

λ	$\overline{g}$	s.d.
413	0.9841	0.0111
443	0.9866	0.0106
490	0.9864	0.0103
510	0.9873	0.0096
560	0.9857	0.0088
620	0.9967	0.0076
665	0.9976	0.0060
681	0.9969	0.0057

$\overline{g}$ is the average over the SIQR; s.d. is the standard deviation of the g population.

population $(g_i)_{i=1,N}$ in order to exclude the possible influence of outliers. Table 1 shows the spectrum of $\overline{g}$ as well as the standard deviation calculated with the entire set of coefficients.

In this exercise, the vicarious gains have been kept at unity for the NIR bands. For SeaWiFS and MODIS, the gain is assumed unity at the longer NIR band and computed at the shorter NIR band so that a maritime aerosol model is selected by the atmospheric correction over targets located in the South Pacific and Indian Ocean subtropical gyres. In this first attempt at presenting a vicarious calibration gain set for the system MERIS+SeaDAS, there is no strong reason to consider g significantly different than 1 at 754 nm. When computing L_t in forward mode with measured L_w, $\overline{g}$ is found equal to 0.9995 and 1.0003 at 754 and 865 nm, respectively. Moreover, the average Ångström exponent α found by MERIS at the MOBY site (average of 1.05, standard deviation, s.d., of 0.43, N=221) is very consistent to that derived from SeaWiFS (1.07, s.d. 0.48) and MODIS onboard Aqua (0.92, s.d., 0.41).

A set of N=102 MERIS scenes fulfill the stringent requirements [25] for computing a vicarious calibration adjustment factor (with 30 in the SIQR). The vicarious calibration adjustment factors depart little from 1, from less than -0.2% in the red to the largest correction of -1.6% at 413 nm (Table 1). The standard deviation of the gain population decreases from 0.011 to 0.006 from blue to red domains, a variability comparable to that found for SeaWiFS (0.009 to 0.007, [25]). As verification, the R_{RS} spectra from MERIS and MOBY have been compared for all available match-ups. Between 413 and 510 nm, the mean absolute relative difference $|\psi|$ varies between 6% and 8%. It is slightly higher (11%) at 560 nm (where R_{RS} is lower), and reaches 62% at 665 nm, a wavelength for which the signal is very near zero.

4. Validation of MERIS reflectance

The location of the 3 AERONET-OC sites used for validation as well as the BiOMaP measurement stations selected as match-ups are displayed on Fig. 1. All statistics are reported in Table 2. Match-ups at 510 nm are fewer or absent because the SeaPRISM 500 nm channel is not always available (see Section 2.3).

4.1. AAOT

The R_{RS} spectra found at AAOT cover a fairly large range of optical conditions [17] and AAOT is thus an informative test site for atmospheric correction schemes. The 194 match-ups found at this site display a relatively good agreement with field data (Table 2, Fig. 2). A few outliers can be seen at the low end of R_{RS} in the blue. Between 490 and 560 nm, $|\psi|$ amounts to 10% with a negligible bias, and r^2 is as high as 0.93-0.95. There are only 90 match-ups at 510 nm

but the statistics are consistent with the neighboring bands, except for a slight increase in *rmsd* (0.00089 sr^{-1}) that might be due to the smaller statistical basis and to uncertainties associated with the band shift correction used to derive a synthetic value of $R_{RS}(510)$ from the SeaPRISM data. The $|\psi|$ value reaches 25% at 413 nm, and 35% at 665 nm. At all wavelengths, the bias does not exceed 6% (except -10% at 665 nm).

The availability of aerosol field measurements at AAOT also allows an assessment of the aerosol model selection by the atmospheric correction, and indirectly of the vicarious calibration in the NIR bands (see Section 3). Comparing the MERIS and field value of α (N=353), $|\psi|$ is equal to 23%, with a negligible bias of 0% (or -0.049 in units of α). In terms of τ_a, $|\psi|$ varies from 28% at 443 nm to 45% at 865 nm, and *rmsd* (in unit of τ_a) from 0.054 to 0.040 for the same bands.

Table 2. MERIS Validation Statistics

AAOT, λ	413	443	490	510	560	665
N	194	194	194	90	194	194
$\|\psi\|$ [%]	25	18	10	10	10	35
ψ [%]	+5	+5	+0	+0	-3	-10
rmsd [10^{-3} sr^{-1}]	1.21	1.02	0.82	0.89	0.72	0.31
GDLT+HLT						
N	85	85	85	-	85	85
$\|\psi\|$ [%]	368	67	20	-	11	17
ψ [%]	+333	+52	+4	-	-3	-9
rmsd [10^{-3} sr^{-1}]	0.81	0.61	0.39	-	0.47	0.19
BiOMaP						
N	100	100	100	100	100	100
$\|\psi\|$ [%]	77	39	15	14	11	19
ψ [%]	+50	+24	+1	-6	-6	-6
rmsd [10^{-3} sr^{-1}]	1.29	0.93	0.70	0.60	0.44	0.17
BiOMaP[1]						
N	55	55	55	55	55	55
$\|\psi\|$ [%]	24	16	12	14	12	23
ψ [%]	-12	-5	-6	-11	-10	-8
rmsd [10^{-3} sr^{-1}]	1.31	0.95	0.85	0.75	0.54	0.21
BiOMaP, Baltic[2]						
N	45	45	45	45	45	45
$\|\psi\|$ [%]	143	67	19	13	9	14
ψ [%]	+126	+59	+11	+1	-2	-4
rmsd [10^{-3} sr^{-1}]	1.27	0.91	0.44	0.33	0.26	0.11

1: without the Baltic stations; 2: only Baltic stations.

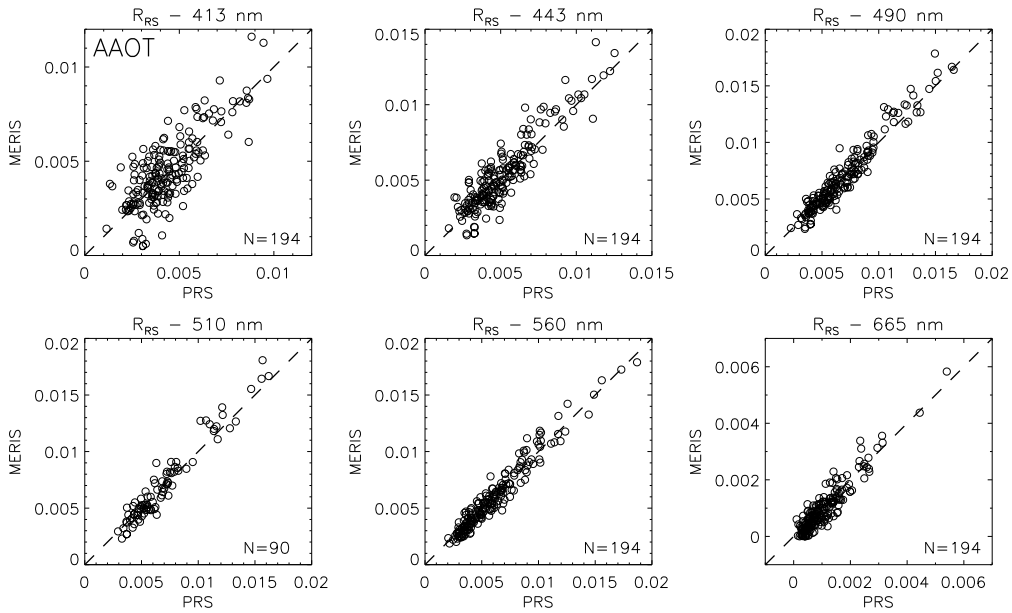

Fig. 2. Comparison of MERIS and SeaPRISM R_{RS} at the AAOT site.

4.2. Baltic sites

The two Baltic sites are associated with 85 match-ups, 43 at GDLT and 42 at HLT (Table 2, Fig. 3). It should be noted that the axes of Fig. 3 cover a range of R_{RS} values that is considerably reduced with respect to Fig. 2. Indeed, R_{RS} found at GDLT and HLT are usually small compared to other water bodies (except in the red) [17]. A consequence is the high values of relative differences in the blue, a spectral domain where R_{RS} found for the match-ups are mostly below 0.002 sr^{-1}. Actually, for these sites the atmospheric correction occasionally returns negative values for $R_{RS}(413)$, and the exclusion of these records by the match-up selection process concurs to shift the distribution of biases at 413 nm towards large positive values. Other elements that might contribute to higher uncertainties in the Baltic Sea include large atmospheric masses associated with high latitudes and the specific bio-optical properties found in the basin. The $|\psi|$ values are lower for longer wavelengths (11% at 560 nm). Still related to the low R_{RS} amplitudes found at the Baltic sites, the spectrum of *rmsd* shows significantly smaller values than those observed at AAOT (as low as 0.00039 sr^{-1} at 490 nm, Table 2).

As for AAOT, the α distribution found at the Baltic sites is almost unbiased with respect to field surface measurements. The relative bias is -1% for the GDLT site (N=85, $|\psi|$ equal to 26%), and +2% for HLT (N=107, $|\psi|$ equal to 30%). The $|\psi|$ values are higher than at AAOT for τ_a, approximately 50% and 75% at 443 and 865 nm, respectively (τ_a for the validation set is significantly lower at the Baltic sites than at AAOT). Based on the analysis conducted with α, the atmospheric correction appears to select a proper representation of the Ångström exponent in different types of atmospheres.

4.3. BiOMaP

The BiOMaP data set yields 100 match-ups distributed in various basins (Fig. 1 and 4), with 45 match-ups in the Baltic Sea (24 and 21 in the northern and southern Baltic Sea, respectively), 22 in the western Black Sea, 15 in the Ligurian Sea, 12 in the eastern Mediterranean and 6 in

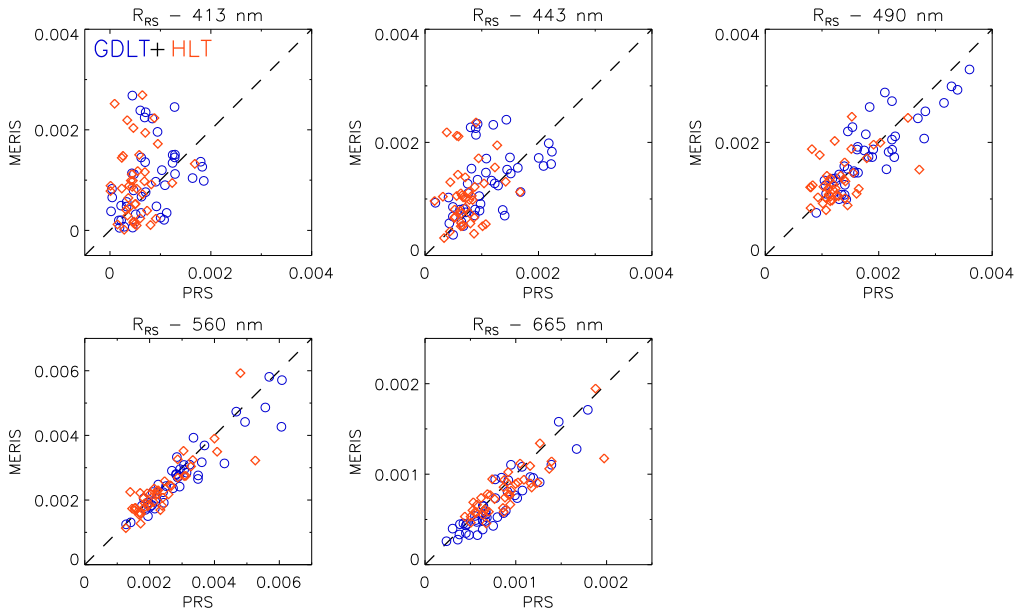

Fig. 3. Comparison of MERIS and SeaPRISM R_{RS} at the GDLT (N=43) and HLT (N=42) sites (blue circles and orange diamonds, respectively).

the English Channel. If Δt is reduced to 3-h, the number of match-ups becomes 64, with $|\psi|$ decreasing by 6% at 413 nm, and 1.0% to 1.6% at the other wavelengths.

From 490 to 665 nm, $|\psi|$ varies between 11% and 19% (Table 2), and is higher in the blue. Large relative overestimates associated with Baltic stations are found in the lower range of R_{RS}. Some of the related stations are located in the Gulf of Bothnia which is characterized by extremely absorbing waters [45]. Considering that almost half the match-ups are found in the Baltic Sea, the comparison statistics are also presented for this subset as well as without the Baltic samples (Table 2). The statistics $|\psi|$ without the Baltic data are very similar to those found at AAOT, from 12% at 560 nm to 23-24% at 413 and 665 nm, but differently the bias is negative across all wavelengths. The 27 match-ups found in the Mediterranean Sea (Ligurian Sea and eastern Mediterranean) display $|\psi|$ of 11-14% between 443 and 560 nm, while $|\psi|$ for the 22 match-ups in the Black Sea is 29% at 412 nm, 18% at 443 nm, approximately 12% at 490 and 510 nm, as low as 8% at 560 nm, and 17% at 665 nm. Both regional subsets show underestimates of R_{RS} at almost all wavelengths (except at 665 nm for the Mediterranean stations, ψ equal to +2%), but they are less pronounced for the Black Sea stations (from -2% to -10% in the domain 413-560 nm). The statistics obtained with the BiOMaP Baltic data share common elements with those found at GDLT and HLT: $|\psi|$ is lowest in the green-to-red spectral domain (as low as 9% at 560 nm) and strongly increases in the blue in relation to large overestimates. The values of *rmsd* are very low for wavelengths longer than 490 nm, decreasing from 0.00044 sr^{-1} at 490 nm to 0.00011 sr^{-1} at 665 nm, while it is comparable to *rmsd* found in the other European basins at 413 and 443 nm (which, combined with low R_{RS} amplitudes, leads to high relative differences $|\psi|$).

4.4. Discussion

Similar validation statistics have been derived for the SeaWiFS and MODIS missions in previous studies [32, 15, 19, 46]). The RMS difference (*rmsd*) is used here as a basis for comparison

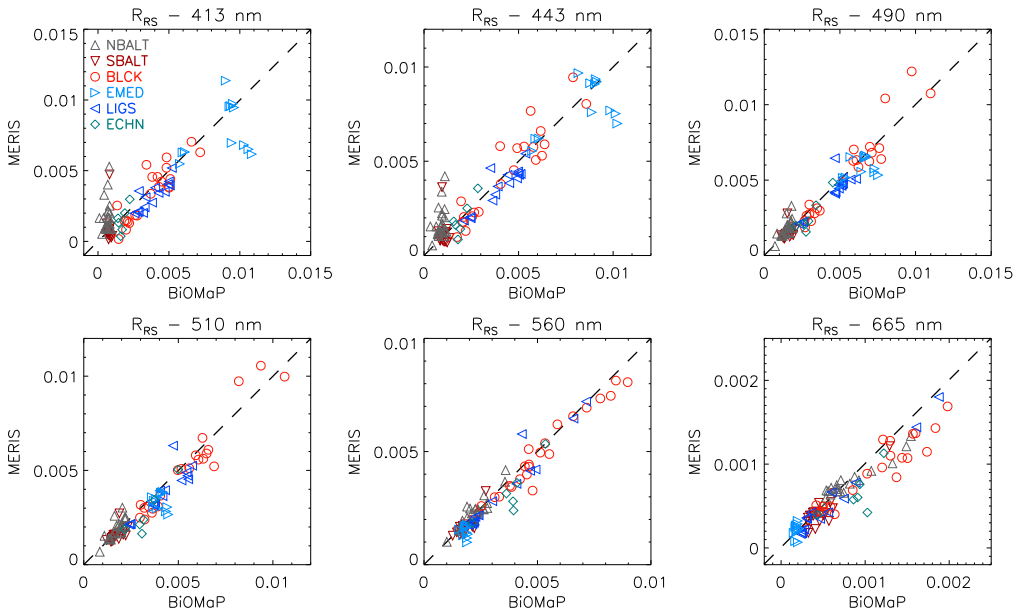

Fig. 4. Comparison of MERIS and BiOMaP R_{RS}. Different colors and symbols are associated with the northern and southern Baltic Sea (NBALT, N=24, and SBALT, N=21), the Black Sea (BLCK, N=22), the eastern Mediterranean (EMED, N=12), the Ligurian Sea (LIGS, N=15) and the English Channel (ECHN, N=6).

since it is less affected by the variations that might be found for relative differences (like $|\psi|$) when R_{RS} amplitudes cover different ranges (particularly when they are low). Fig. 5 shows *rmsd* found for the three match-up subsets described here and for the three satellite missions as obtained with consistent selection criteria over similar time periods. For the AAOT set, there is a local maximum observed in *rmsd* for MODIS at 531 nm, which might be at least partly due to the lower number of match-up points at that wavelength (201 versus 486 for the other wavelengths) and to the band shift correction that relies on SeaPRISM records at approximately 500 and 550 nm [47]. The results for that band are thus to be taken with more caution.

Generally, the *rmsd* curves obtained for the three missions appear relatively consistent, even though some differences can be noticed and at least partly explained by the differences in the match-up sets as well as the various elements that are specific for each mission in terms of sensor design, observation geometry or processing code. The lowest values are usually shown for the Baltic sites GDLT and HLT, and the highest for AAOT. The *rmsd* spectra are broadly contained in an envelop decreasing from 0.0008-0.0015 sr^{-1} at 412-413 nm to 0.0002-0.0004 sr^{-1} in the red. The results obtained at corresponding bands can be compared for the 3 sensors using the letters M, A and S as superscripts for MERIS, MODIS and SeaWiFS, respectively. The ratio of *rmsd* associated with MERIS and MODIS (i.e., $rmsd^M/rmsd^A$) is in the interval 0.69-0.83 for the Baltic sites (i.e., *rmsd* lower for MERIS), and in the interval 0.81-1.25 for the 2 other data sets, being noticeably larger than 1 only at 412 nm (1.25) in the case of BiOMaP. If the Baltic stations are excluded from the BiOMaP data set, this ratio is between 0.96 and 1.17. The *rmsd* found for SeaWiFS tends to be higher than for MERIS or MODIS, which might be explained by a lower signal-to-noise ratio for that mission. The ratio of *rmsd* associated with MERIS and SeaWiFS ($rmsd^M/rmsd^S$) is mostly in the interval 0.64-0.84, except 0.58 for $rmsd^M(560)/rmsd^S(555)$ at AAOT, and approximately 1 for $rmsd^M(560)/rmsd^S(555)$

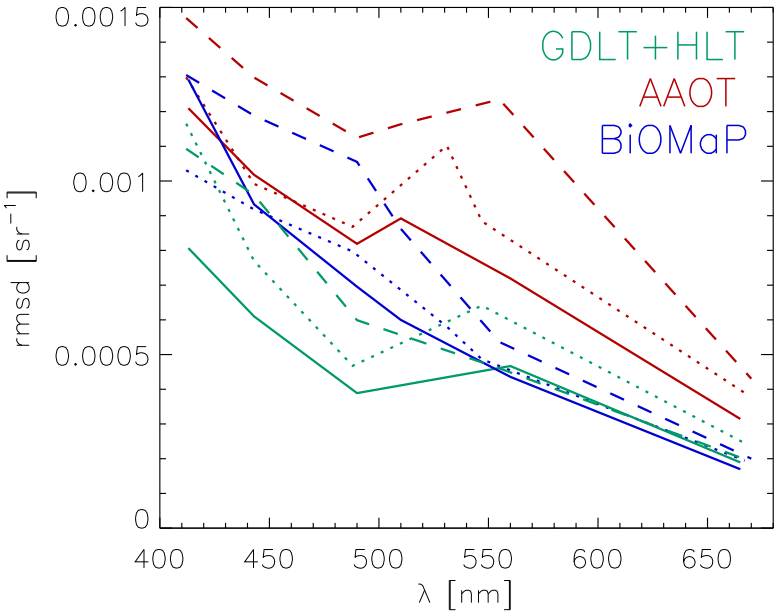

Fig. 5. Spectrum of the RMS difference for MERIS (continuous line), MODIS (dotted line) and SeaWiFS (dashed line) for the three match-up subsets. For the GDLT and HLT sites, AAOT and BiOMaP, the total number of match-ups is 236 (not plotted at 531 nm), 486 (201 at 531 nm) and 155 for MODIS, and 67, 484 (250 at 510 nm), and 147 for SeaWiFS.

and $rmsd^M(665)/rmsd^S(670)$ for the Baltic sites, and $rmsd^M(413)/rmsd^S(412)$ for the BiOMaP validation set. The ratio associated with BiOMaP considered without its Baltic stations is in the interval 0.73-1.01. Overall using the *rmsd* metric, the uncertainties associated with MERIS are generally comparable with those of MODIS and lower than those of SeaWiFS.

5. Conclusion

This work is an early assessment of the use of SeaDAS to process MERIS imagery. A set of vicarious calibration coefficients has been derived at the MOBY site, which was used for the same purpose for SeaWiFS and MODIS. Using this set of coefficients is recommended for processing MERIS imagery with SeaDAS (version 6.2). The validation data are associated with measurements collected in the European seas and cover a large gradient of optical properties, from oligotrophic areas to coastal sediment-dominated or CDOM-dominated waters. While recognizing that the accuracy of the atmospheric correction should still be improved, the encouraging results documented here provide a solid ground for future developments aiming at fine-tuning the MERIS+SeaDAS system.

Excluding the Baltic Sea, the mean absolute relative difference $|\psi|$ is between 10% and 14% for the spectral interval 490-560 nm, 16-18% at 443 nm, and 24-26% at 413 nm. The $|\psi|$ values are much higher for Baltic waters for the blue bands, but similar or lower at 560 and 665 nm. The validation statistics presented here show differences lower than those documented for MERIS R_{RS} derived from the MEGS version 7.4 processor [30, 48, 49, 50]. These differences are likely to be affected by a recent update (MEGS version 8 [51]) that includes vicarious calibration performed with in situ data from two target sites (MOBY and the BOUSSOLE

system in the Ligurian Sea [52]).

Importantly, the present validation results document uncertainties that appear at least as good as those associated with SeaWiFS and MODIS. The *rmsd* values given here for MERIS as well as those documented for SeaWiFS and MODIS, are required information to generate merged records of R_{RS} [53, 2, 54]. With a view on creating a multi-sensor data stream for the European seas, this works leads to processing imagery collected by the major ocean color satellite missions with a common processing environment producing ocean reflectance spectra of very comparable accuracy.

Acknowledgements

This work is contributing to the Ocean Colour Climate Change Initiative (OC-CCI) of the European Space Agency. The authors wish to thank the AERONET team members for their continuous effort in supporting AERONET-OC. MOBY is currently supported by NOAA.